Improved superconducting hot-electron bolometer devices for the THz range

T.M.Klapwijk[a], R.Barends[a], J.R.Gao[a,b], M.Hajenius[a,b], and J.J.A.Baselmans[b]

[a]Kavli Institute of Nanoscience, Faculty of Applied Sciences, Delft University of Technology, Lorentzweg 1
2628 CJ Delft, The Netherlands
[b]Space Research Organisation of the Netherlands, Sorbonnelaan 2, 3584 CA Utrecht, The Netherlands

ABSTRACT

Improved and reproducible heterodyne mixing (noise temperatures of 950 K at 2.5 THz) has been realized with NbN based hot-electron superconducting devices with low contact resistances. A distributed temperature numerical model of the NbN bridge, based on a local electron and a phonon temperature, has been used to understand the physical conditions during the mixing process. We find that the mixing is predominantly due to the exponential rise of the local resistivity as a function of electron temperature.

Keywords: Hot electrons,heterodyne mixing,terahertz

1. INTRODUCTION

In the past decade a great deal of progress has been made to achieve low noise heterodyne detection at frequencies beyond 1.4 THz. The physics is based on "hot electrons", meaning electrons at an elevated electron temperature, which translates into an observable change in resistance. In contrast to semiconductors, in metals the resistance is only weakly dependent on temperature. However, in superconducting metals the resistance is very strongly dependent on temperature around the critical temperature T_c. It was demonstrated by Gershenson *et al*[1] that the response and decay time of electrons in metals can be very fast, suggesting the possibility of creating fast detectors based on superconducting films. Recently, we have demonstrated that such devices can be made in a reproducible manner with excellent performance up to frequencies of 2.5 THz.[2] Since this improvement in performance has been realized predominantly by changing the devices a careful analysis of the device physics under operating conditions is needed. In this contribution we focus on the relationship between material properties and device properties under operating conditions.

We will first review the crucial parameters which influence, in one way or another, the device properties and their performance. After a description of the realized devices a numerical analysis is used to understand their response under operating conditions. We end with some recommendations.

2. CRUCIAL PARAMETERS

2.1. Resistive transition

The temperature dependence of the resistance of a superconductor around its critical temperature T_c, the so-called resistive transition, has been well studied.[3] In highly resistive 2-dimensional films the behavior is controlled by the Kosterlitz-Thouless phase transition, which leads to a broadening of the transition for increasing intrinsic resistance of the films in the normal state.[4] Upon approaching T_c vortex-antivortex pairs start to dissociate, leading to free vortices, which under the influence of a transport current are driven by the Lorentz force manifesting itself as resistance. The width of the transition will broaden considerably for resistances per square of the order 10 $k\Omega$. For resistances used for bolometers (600 Ω to 900 Ω) this is a

Further author information:
E-mail: klapwijk@tnw.tudelft.nl, Telephone: 0031152782600

Millimeter and Submillimeter Detectors for Astronomy II, edited by
Jonas Zmuidzinas, Wayne S. Holland, Stafford Withington, Proceedings of
SPIE Vol. 5498 (SPIE, Bellingham, WA, 2004) · 0277-786X/04/$15 · doi: 10.1117/12.552916

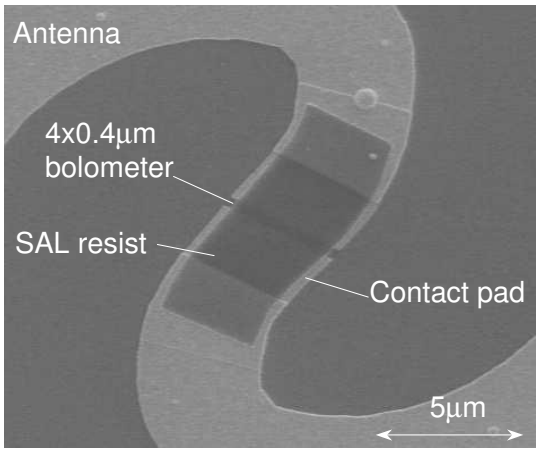

Figure 1. Top view of a device (of 4 μm by 0.4 μm) integrated in a spiral antenna. The spiral antenna is made of Au, which overlaps with the underlying NbN film. In practice the active NbN part of the devices can be shorter and narrower compared to the width of the antenna.

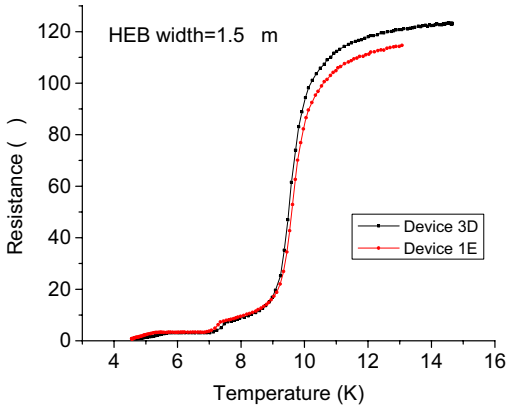

Figure 2. Typical resistance as a function of temperature curves(for twin-slot antennas). Note the similarity for two different devices. The step like structure at the lower temperatures reflects the influence of the contacts and the leads, which each have a slightly lower critical temperature.

negligible effect and the resistance emerges due to the thermal creation of vortices. In addition it is possible that the resistive transition is partially influenced by extrinsic properties such as spatial inhomogeneities of the T_c of the film. Fig.2 shows typical resistive transitions for our devices. The sharp drop in resistance around 9.5 K is due to the NbN film. The structure at lower temperatures is device-specific.

Used as a THz detector the superconducting film is connected to a highly conductive antenna, usually Au. Hence, fully normal currents will be converted into supercurrents. This phenomenon leads to an additional resistive contribution which influences the observed resistive transition. It has been emphasized by Wilms Floet *et al*[5] and compared with niobium bolometers. More recently an improved and detailed analysis has been made using aluminium by Boogaard *et al*.[6] Fig. shows the resistive transition for aluminium wires between normal metal contacts. For different wire-lengths one finds a scaling of the resistances in the normal state. However, all curves get the same remaining resistance at the lower temperatures. It has been demonstrated that this is intrinsic and due to the conversion of normal currents to supercurrents, which leads to a resistive contribution at both ends with a length of the order of the coherence length. Note also that the T_c is also depressed for different wire-lengths. The consequence is that a superconducting wire is resistive over a length of the coherence length even for fully clean interfaces. Obviously, this leads to a deteriorated dR/dT compared to the intrinsic one of the superconducting film, although the influence on the detector response is non-trivial. The consequence is that the resistivity of the superconducting film connected to normal metal leads is position-dependent over a length of the order of the coherence length (for Al we used 124 nm; for NbN it is only 4 nm at low temperatures).

2.2. Response times

The response time of the electron gas is in principle determined by the electron-phonon interaction time. It is assumed that electron-electron interaction is fast enough to allow a thermal distribution to be established at an elevated temperature. The electrons relax their energy to the phonon bath and the phonons escape to the substrate or diffuse out of the film into the leads. In early experiments it was found that the response time of niobium leads to a maximum response time of only 100 MHz, which is the limiting bandwidth for the intermediate frequency (IF) signal in a heterodyne experiment. Subsequently, research has been focused on thinner films (to shorten the phonon escape time) and to materials with a stronger electron-phonon

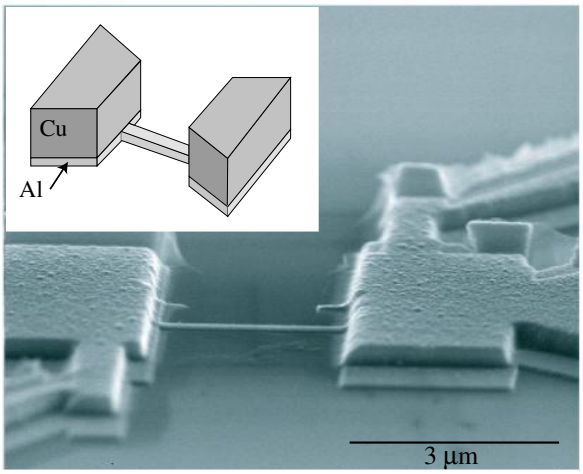

Figure 3. SEM picture of a device (slightly misaligned), showing the coverage of the thin aluminium film with the thick Cu layer. The inset shows a schematic picture of an ideal device.

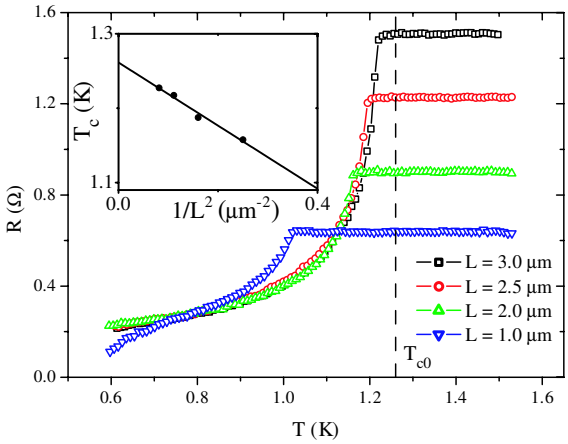

Figure 4. Measured $R-T$ curves for four different bridge lengths. The intrinsic T_{c0} is indicated by the vertical dashed line. The inset shows the measured critical temperature of the wire *vs* $1/L^2$, which is used to determine T_{c0} by letting $L \to \infty$.

interaction (i.e. superconducting materials with a higher T_c. Currently, NbN has become the dominant workhorse, although other materials have been proposed.[7]

As an alternative to engineer the response time the concept of diffusion-cooling has been introduced by Prober.[8] Connecting the superconducting film to leads in equilibrium leads to a response time given by $\tau_D \sim L^2/D$ the diffusion time for electrons over a length of the bridge L. To increase the response time the bridge should be as short as possible and the diffusion constant as large as possible. The consequence is that the resistive transition becomes more and more dominated by the conversion processes and becomes less and less dependent on the intrinsic properties of the superconductor(see Section 2.1).

2.3. Lumped circuit and distributed temperature

The time-dependent response and the noise have been mostly analyzed with a so-called lumped circuit model. The superconducting film is taken as a homogeneously heated object with a given resistive transition.[9–11] In practice, as discussed above, the superconducting film is connected to normal metal leads which poses a boundary condition for the spatially dependent heat balance equation. Such a distributed model has been used by Araujo and White,[12] Wilms Floet *et al*,[13] and Merkel *et al*.[14] It is assumed that the functional relation between the resistance as a function of temperature is homogeneous throughout the active volume. Then it is sufficient to know the position-dependent temperature $T(x)$. Knowing $T(x)$ together with the temperature-dependent resistivity $\varrho(T)$ the resistivity at each point in the device is known.

Since for a diffusion-cooled device the resistive transition is not a material property but the result of the geometry and the conversion of normal current into a supercurrent even for a uniform temperature the resistivity is a function of position. A temperature profile is therefore the result of power dissipation heating at the edges and power dissipation in the middle, which renders the diffusion-cooled device in one, which is difficult to model and very sensitively dependent on fabrication details. The experimentally observed poor reproducibility and the progress in phonon-cooled devices has led recently to an emphasis on phonon-cooled devices. Assuming that the fabrication can be controlled adequately the material determines the resistive transition and the resistance of the active volume is directly related to the resistive transition. For such a device $\varrho(T)$ can be inferred from the measured intrinsic properties of the resistive transition and used as input for the modeling based on a local electron temperature $T(x)$.

2.4. Biasing method

The hot-electron bolometers are all based on using the voltage response to a small increase in temperature. Hence, in principle one would like to bias the device at a temperature where dR/dT is large,[8] which means at an electron temperature close to T_c. Devices are always operated at a phonon-temperature far below T_c. The operating point close to T_c is reached by passing a large dc current through the device. This has led Wilms Floet *et al*[5] to an analysis of the state that arises in a superconducting bridge for a high dc current. They modified the SBT-model[15] for hot-spot formation in a superconducting microbridge by focusing on an *electronic* hot spot. They subsequently proposed an alternative concept for mixing[13] in which the temperature rise modulates the length of a fully normal domain.

In practice bolometer mixers are brought to their operating point by applying sufficient LO power to raise the temperature to close to T_c. Fig. 5 shows a typical set of current-voltage characteristics for different LO powers for devices shown in Fig.1 together with noise temperatures at 2.5 THz. Fig.6 shows a more detailed set for the smaller devices. The center region indicates the region of optimum sensitivity. Using the LO to bias the device to a temperature close to the critical temperature was proposed by Karasik and Elantiev[10] and analyzed in a distributed temperature model by Araujo and White[12] for diffusion-cooled bolometers (although the principle can be applied to phonon-cooled as well[16]). In the current generation of phonon-cooled devices optimum bias conditions are found for LO power about one order of magnitude larger than the applied dc power. For example in Fig.6), optimal DC bias is for about 10 nW, whereas the applied LO power is about an order of magnitude larger.

2.5. Device size and LO power requirements

Obviously, for diffusion-cooled devices a fast response can only be realized with very short devices. For phonon-cooled devices the critical quantity is the needed LO power. In a lumped circuit model Karasik and Elantiev[10] derived:

$$P_{LO} = \frac{1}{\alpha} AV(T_c^n - T^n - nT_c^{n-1}\Delta T_c) \tag{1}$$

with V the film volume, A and n material dependent constants ΔT_c the width of the resistive transition and α the coupling factor of radiation to the mixer. T is the bath temperature and it is assumed that P_{LO} is capable of heating the electron gas to the critical temperature of the bridge. In this expression it is assumed that the phonon temperature equals the bath temperature. The demands for a fast response has led to the use of very thin NbN films (3.5 nm thick). A further reduction in volume is achieved by working with narrow and short (to assure impedance matching) devices, which allows compatibility with the current generation of solid state LO's.[17]

2.6. Electron and phonon temperature

On a mesoscopic length scale it becomes increasingly more difficult to use concepts as electron temperature and phonon temperature. Pothier *et al*[18] have clearly shown that an electron temperature can only be defined for samples longer than the electron-electron interaction length $\sqrt{D\tau_{ee}}$. They find for normal metal wires with perfect contacts to the equilibrium reservoirs that the energy distribution is given by a Fermi-function with a local chemical potential of $\mu(x) = -eUx$ with U the voltage difference between the reservoirs, x the coordinate along the wire and an effective temperature given by:

$$T_{eff} = \sqrt{T^2 + x(1-x)\frac{U^2}{L}}. \tag{2}$$

L is the Lorentz number $\pi^2 k_B/3e^2$ for a free electron gas. For shorter lengths a two-step distribution function is found reflecting the distribution functions in the reservoirs at different voltages. For our NbN $\sqrt{D\tau_{ee}} = 8nm$ and a thermal distribution is a reasonable assumption.

The limits of a description in terms of a phonon temperature is less well-established. Acoustic waveguide modes have been invoked to interpret experiments on metallic wires by Seyler and Wybourne.[19] In crystalline

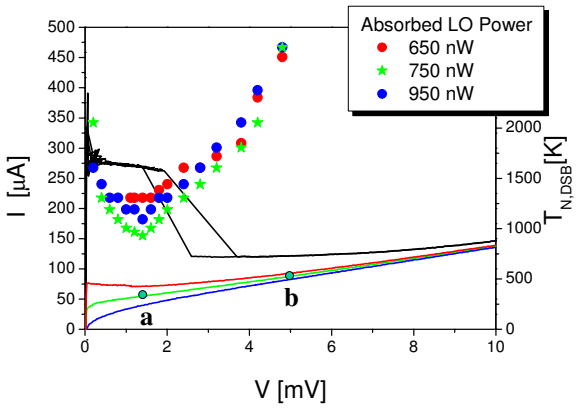

Figure 5. Current-voltage characteristics for different LO powers and the measured heterodyne response, expressed in noise temperatures, for devices shown in Fig.1

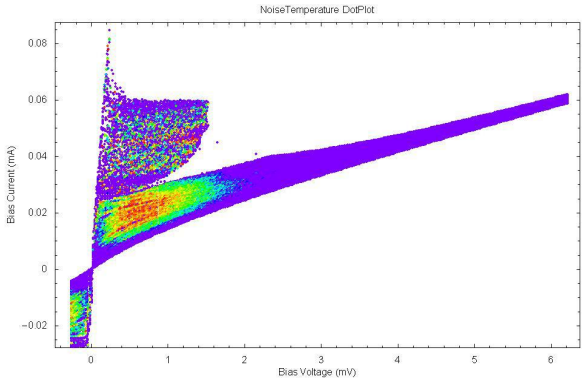

Figure 6. Current-voltage characteristics for smaller devices. The color indicates the strength of the heterodyne response for various bias levels.

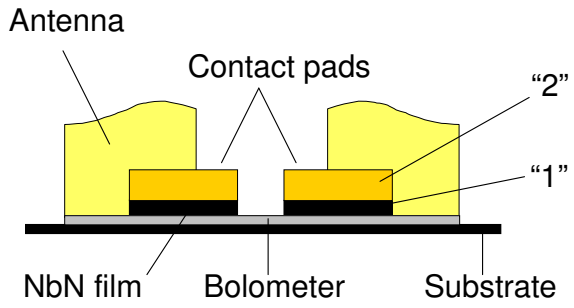

Figure 7. Cross-section of a typical device. Before depositing the Au antenna the NbN is sputter-cleaned followed by depositing a thin layer of NbTiN (15 nm) and Au layer. The antenna is deposited in the next step on the clean Au surface.

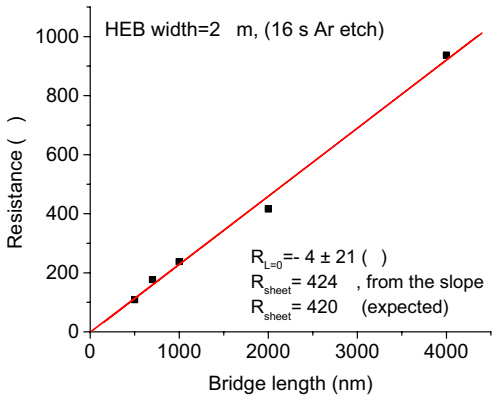

Figure 8. Normal state resistance, measured at 16 K, of a number of devices of various bridge lengths. Evidently, the contact resistances are negligible.

and amorphous dielectrics of mesoscopic sizes a description has emerged using radiative thermal transport in solids.[20] Ballistic phonons are used, analogous to the description of the Kapitza resistance in terms of scattering of phonons at solid-solid interfaces. A Landauer-type description has been developed emerged[21, 22] and used to interpret experiments on crystalline silicon.[23] In a Landauer-description the mesoscopic sample is connected to leads which act as equilibrium reservoirs emitting phonons in the wire. A quasi-equilibrium phonon temperature is then no longer a valid concept. Nevertheless, we will use such a concept below in order to demonstrate that the phonon heat bath can not be ignored in understanding the quantitative details of the hot-electron bolometer mixers.

3. DEVICES

Promising results have been reported for phonon-cooled devices since the original proposal by Gershenson *et al.*[9] A major improvement was the introduction of thin films of NbN by Gol'tsman *et al.* We report on results obtained for phonon-cooled devices based on these films for use from 1.4 THz to 2.5 THz. Films with a sheet resistance $R_{\square}$ of 600Ω, thickness of 3.5 nm, a resistivity ϱ of 210$\mu\Omega cm$ and a T_c of 9.3 tot 9.9 K, have been incorporated in an antenna. Both wide-band (spiral) and narrow-band (twin-slot) antenna's have

been used. We have found[2, 24] that a critical factor is the contact between the Au antenna's and the NbN films. Fig.7 shows a cross-section of the devices. The NbN films have been exposed to air for a prolonged period of time before subsequent lithographic patterning is done. The surface of the NbN is cleaned with an Ar sputter etch followed by depositing either a Au/Ti layer or a NbTiN layer followed by a Au layer. This sputter clean procedure leads to a deterioration of the quality of the NbN, *i.e.* a lowering of T_c. The introduction of a NbTiN interfacial layer is introduced to avoid a reduction of the T_c of the NbN under the Au pads. Importantly, in contrast to results reported before the normal state resistance of the devices scales with the geometrical dimensions of the bridge(Fig.8) and are in agreement with the expected values based on the $R_\Box$ of the films. The coherence length ξ of the NbN film is about 4 nm, which implies that an intrinsic boundary resistance (Subsection 2.1) could only contribute less than 10 % of the remaining resistance. In previous experiments a large value for the interfacial resistance, due to the fabrication technology, had to be assumed, which influences the device behavior and device modeling considerably. Most importantly, the devices with the NbTiN interfacial layer showed superior device performance (Figs.5,6).

Table 1. Summary of results obtained with a twin slot antenna. The bridge width is $1\mu m$. The critical current is the maximum current value observed for no applied LO power. The LO frequency is the actually applied frequency and T_N is the observed noise temperature for heterodyne mixing. Two values of the LO power at optimum bias are listed. The first is inferred from the current-voltage characteristic, called the isothermal technique, the second is measured from the LO source. Existing discrepancies are not yet clarified, but we assume that about $100nW$ is actually absorbed by the device.

Device	**Twin slot**	**Length**	$I_c(4K)$	**LO Frequency**	T_N	P_{LO} isothermal	P_{LO} at lens
M6T-3K	1.6 THz	0.15 μm	73 μA	1.63 THz	910 K	40 nW	220 nW
M6T-2K	1.6 THz	0.15	70	1.63	960	30	170
M6T-1K	1.6 THz	0.15	50	1.63	980	30	170
M6T-11K	1.8 THz	0.15	50	1.89	940	30	170
M6T-9L	1.8 THz	0.10	68	1.89	1030		
M8T-H1	1.8 THz	0.15	90	1.89	990	70	390
M9T-C3	1.6 THz	0.20	90	1.63	930	90	500

4. PERFORMANCE

The devices with these improved contact allowed the design and fabrication for impedance matched twin slot antenna mixers. The results are summarized in Table 1. Details are given in the paper by Baselmans *et al.*[25] The Table clearly shows that the devices show very comparable performance. In addition the needed LO power is a factor of 2 to 4 less than for the larger devices(Fig.1) reported before.[2]

5. ANALYSIS

The systematic and reproducible behavior reported in Sections 3 and 4 suggests that the material and device parameters controlling the bolometer response are well under control. It is striking that under optimum bias conditions $P_{LO} \gg P_{DC}$. We have made a crude analysis of the resistive transition for increasing values of P_{LO} and find that it is initially a shift of an undistorted resistive transition to lower temperatures indicative of an enhancement of the electron temperature with P_{LO} until it reaches the critical temperature of the material. So we assume that the bias conditions, raising the electron temperature by the LO power until the critical temperature is reached, envisioned by Karasik and Elantiev[10] apply.

We will analyze the results using a distributed temperature model, analogous to the one introduced by Araujo and White.[12] We assume a one-dimensional model. This is justified on the basis of the expected

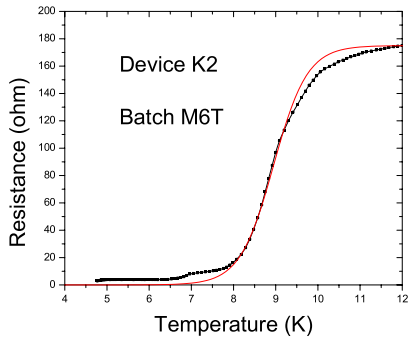

Figure 9. Resistive transition (dots)for a particular device compared with the Fermi function(Eq.6)(full line). Apart form small deviations at the lower temperatures it is assumed that this curve represents the intrinsic local resistivity of the NbN film with $T_c = 8.95K$ and $\Delta T = 0.4K$.

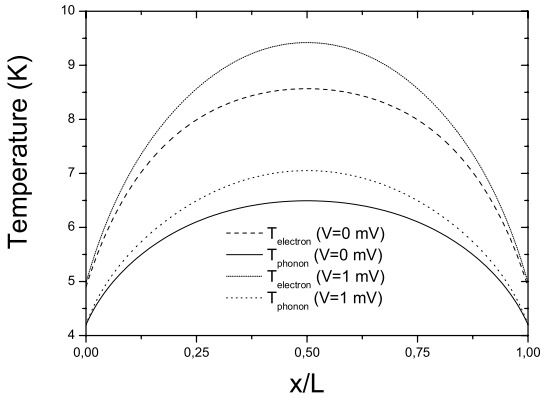

Figure 10. Electron and phonon temperatures as a function of position for two different values of the DC bias voltage. The T_c, the mid-point of the resistive transition, is equal to 8.95 K. The applied LO power is $80nW$.

current-distribution. For the given material properties of NbN the penetration-depth $\lambda_\perp$ is at 4.2 K equal to 1.2 μm and increases with increasing temperature. Hence, we may assume a uniform current-density over the cross-section. However, in principle we should allow for variation of the order parameter over the cross-section and the formation of vortices, in view of the small value of the coherence length compared to the cross-section. Since we will work in practice well into the resistive transition, close to the mid-point of the transition T_c, we assume that the formation of vortices will play a negligible role under operating conditions.

Two coupled heat balance equations are used, one for the electron temperature T_e and one for the phonon temperature T_p. As argued in Subsection 2.6 the concept of a local electron temperature is reasonable. At the operating point the temperature the wavelength of a thermal phonon is about 30 nm, clearly much thinner than the thickness but still smaller than the length of 150 nm. Therefore we assume that a local phonon temperature is a fair assumption at the temperatures used. The bridge has a length L, a width W and a layer thickness d. The effect of the contacts is present via the boundary conditions. For the differential equations we use:

$$\begin{aligned} \frac{\partial}{\partial x}(\lambda_e \frac{\partial}{\partial x} T_e) + p - p_{ep} = 0, \\ \frac{\partial}{\partial x}(\lambda_p \frac{\partial}{\partial x} T_p) + p_{ep} - p_{ps} = 0, \end{aligned} \tag{3}$$

with λ_e and λ_p the heat conductivity for the electrons and phonons respectively. The functions p represent the power absorption or generation per unit volume. We assume homogeneous power absorption from the LO because $\hbar\omega \gg 2\Delta$ and a position dependent power-generation for DC. Hence, $p = p_{RF} + p_{DC}$ with $p_{DC} = J^2\rho$ dependent on the local value of ρ. The transfer from the electron bath to the phonon bath is indicated by p_{ep}. The transfer from phonons to the substrate is indicated by p_{ps}. Both p_{ep} and p_{ps} are assumed to be uniform through the bridge apart from their temperature dependence[26,27]:

$$\begin{aligned} p_{ep} = g_{ep}(T_e^n - T_p^n) \\ p_{ps} = g_{ps}(T_p^m - T_b^m) \end{aligned} \tag{4}$$

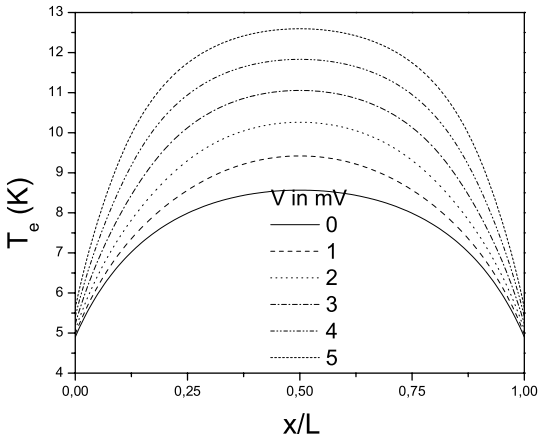

Figure 11. Various electron temperatures along the bridge for a range of DC biases($PLO = 80\ nW$). Note that the temperature exceeds the critical temperature of the NbN.

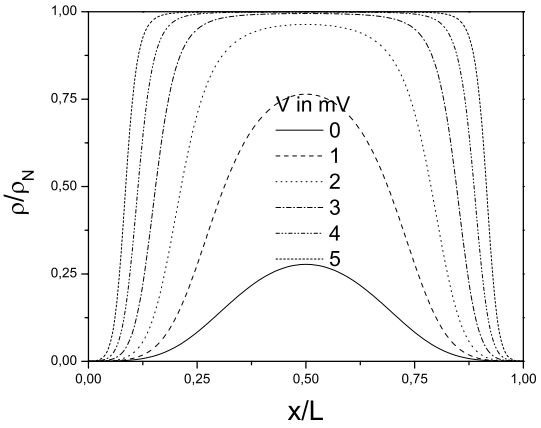

Figure 12. Local resistivity which develops in response to the electron temperature profile given in Fig.11. The two bell-shaped curves in the middle represent the conditions under which mixing is most effective.

with the prefactors given by:

$$g_{ep} = \frac{c_e}{n\tau_{ep}T_e^{n-1}}$$
$$g_{ps} = \frac{c_p}{m\tau_{esc}T_p^{m-1}} \tag{5}$$

With $n = m = 4$, $c_e = \gamma_e T_e$, $c_p = \gamma_p T_p^3$, $\tau_{ep} = \frac{\tau_{epf}}{T_e^2}$ and τ_{esc} temperature independent, g_{ep} and g_{ps} become independent of temperature.

We approximate the $R(T)$ curve, following Araujo and White[12] by a Fermi-function:

$$\rho(T) = \frac{\rho_n}{1 + e^{-\frac{T-T_c}{\Delta T_c}}} \tag{6}$$

which represents the local resistivity for a given local electron temperature T_e with ρ_n the resistivity in the normal state and ΔT a device dependent parameter. It assumes that from the device all the resistance is due to the NbN and ignores other contributions. The temperature T_e is found from solving these two coupled differential equations for the electron temperature T_e and the phonon temperature T_{ph}. Fig.9 shows the resistive transition for a particular device and a comparison with Eq.6. Obviously, Eq.6 describes the observed resistive transition quite well and in this case with $T_c = 8.95K$ and $\Delta T - 0.4\ K$.

At the boundaries we assume the phonon temperature T_p to be equal to the bath temperature (set at $4.2\ K$, since it is close to a large pad. For the electron temperature T_e the situation is more complicated. The electronic heat flow at the boundary is constant. The electrons carrying this heat can diffuse into NbTiN and Au layers(Fig.7, yet at the contacts there is a possible finite interface transparency T_r (in the order of 5 %.[24] We assume that under the contacts the electron temperature decays exponentially, with a decay length l. At the boundary at $x = 0$ we then have:

$$T_p(x = 0) = T_{bath}$$

$$T_e(x<0) = \Delta T e^{x/l} + T_{bath}$$
$$\frac{d}{dx}T_e(x=0) = \frac{\Delta T}{l} \tag{7}$$

with $\Delta T = T_e(x=0) - T_{bath}$. The length l is given by

$$l = \sqrt{\frac{R_c}{R_\square}} \tag{8}$$

with R_c the contact resistance per unit area.

Fig.10 shows a typical result of the electron and phonon temperatures for 0 mV DC bias and 1 mV. Obviously the electron temperature is considerably higher than the phonon temperature, partly because of the differences in boundary conditions. Note that the increased DC bias has only a minor influence on the temperature profile (the applied LO power is $80nW$). Fig.11 shows a set of electron temperatures for a larger range of DC bias voltages. Most importantly is the result shown in Fig.12. For 0 mV DC bias a bell-shaped curve is obtained in the middle of the bridge. At these electron temperatures the local resistivity inferred from Eq.6 becomes significant and rises sharply with increasing DC voltage. Hence, although the temperature change is minor the contribution to the height of the local resistivity is considerable. Upon further increase of voltage, outside the operating range of the mixers, the bridge becomes fully normal and could have been called a normal hot spot.

In the numerical modeling we have used numbers which are as close as possible to the devices of which results are shown in Fig.6 and Table 1. At the operating point the voltage is less than 1 mV and resistivity at the center is still substantially below the normal state resistivity. Figs.13 and 14 show predictions for the current-voltage characteristics and the resistance values for different LO powers. The overall shape is in agreement with what is observed experimentally. Note that Fig.14 shows that for P_{RF} of 80 nW the total resistance of the NbN bridge is only of order 10 % of the normal state resistance. This is an important observation which has to guide further modelling and device development. It means that the resistance of the bridge is under operating conditions comparable to the remaining resistance of the contacts (Fig.9. Hence, we can no longer assume that the resistivity is locally identical and our heat balance equation must include sources of extra dissipation at the contacts. Although, a finite transparency of the contacts has been assumed for the heat balance equation it was not yet included as an additional source of power dissipation.

6. DISCUSSION AND CONCLUSIONS

Improved bolometer devices have been realized with superior mixing performance suitable for the 1.4 tot 2.5 THz range. Most of the device parameters can be technologically controlled allowing design-optimization of device impedance and antenna. Based on a realistic model we find that the devices work in a regime where the resistance is due to a LO-power induced bell-shaped resistivity curve in the center of the NbN bridge(Fig.12), which is exponentially dependent on a temperature rise. We also find that in this regime the devices, although with a negligible contact resistance in the normal state, still suffer from remnants of the contact resistance appearing at the temperatures of operation. Further experimental work is needed to remove the remaining contact resistance, such as developing devices analogously to those used by Karasik *et al.*[28] Apart from improved performance it would enable a complete numerical analysis of the response. Clearly, understanding this delicate interplay between heat-flow. contact resistances, temperature distribution and local resistivity is crucial. It will also be needed to understand the absorbed LO power quantitatively, the stability and the ultimate sensitivity.

7. ACKNOWLEDGMENTS

We thank the European Space Agency and NanoImpuls for financial support, M.E.Gershenson for helpful suggestions and P.A.J.de Korte for stimulating interest.

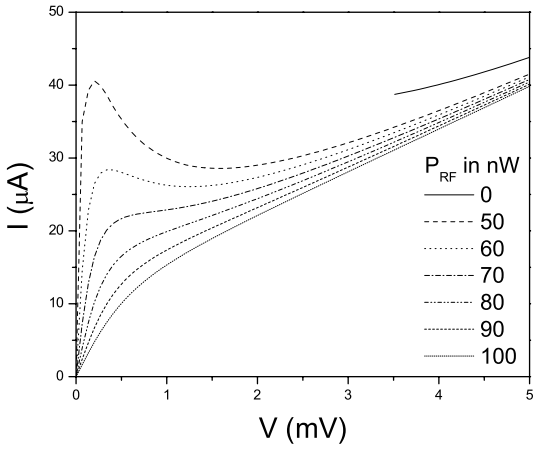

Figure 13. Typical current-voltage characteristics for various values of applied LO power.

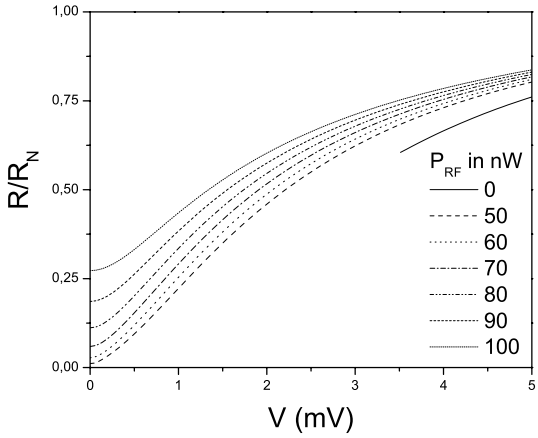

Figure 14. Resistance as a function of voltage for various values of LO power. Note the absolute value of the resistances compared to the normal state resistance at DC bias values below $1mV$ the range of practical interest.

REFERENCES

1. E.M.Gershenson,M.E.Gershenson, G.N.Gol'tsman, A.D.Semenov, and A.V.Sergeev, Sov.Phys. JETP **59**, 442 (1984)
2. J.J.A.Baselmans, M.Hajenius, J.R.Gao, T.M.Klapwijk, P.A.J. de Korte, B.Voronov, and G.Gol'tsman, Appl. Phys. Letters, **84**, 1958 (2004)
3. W.J.Skocpol and M.Tinkham, Reports on Progress in Physics, **38**,1049(1975)
4. M.R.Beasley, J.E.Mooij, and T.P.Orlando, Phys. Rev. Letters, **42**1165(1979); S.Doniach and B.A.Huberman, Phys.Rev.Letters, **42**1169(1979);B.I.Halperin and D.R.Nelson,J.Low Temp Phys, **36**, 599 (1979)
5. D.Wilms Floet, J.J.A.Baselmans, T.M.Klapwijk and J.R.Gao, Appl.Phys. Letters, **73**,2826 (1998)
6. G.R.Boogaard, A.H.Verbruggen, W.Belzig, and T.M.Klapwijk, to be published in Phys. Rev.B, Rap Comm, 2004;cond-mat/0401364v2
7. B.S.Karasik, W.R.McGrath, R.A.Wyss, Optimal choice of materials for HEB superconducting mixers. IEEE Transactions on Applied Superconductivity, **9**, 4213 (1999)
8. D.E.Prober, Appl. Phys. Letters **62**,2119(1993); see also earlier related work of M.Tinkham, M.Octavio and W.J.Skocpol, J.Appl. Phys.**48**,1311 (1977)
9. E.M.Gershenson, G.N.Gol'tsman, I.G.Gogidze, Y.P.Gusev, A.I.Elant'ev, B.S.Karasik, and A.D.Semenov, Superconductivity **3**,1582(1990)
10. B.S.Karasik and A.I.Elantiev, Appl. Phys. Lett., **68**,853(1996)
11. Phys. Rev. **B28**,5150(1983)
12. H.Araujo and G.J.White, IEEE Trans on Applied Superconductivity, **9**,4229 (1999)
13. D.Wilms Floet, E.Miedema, T.M.Klapwijk and J.R.Gao, Appl. Phys. Letters **74**, 433 (1999)
14. H.Merkel, P.Khosropanah, D.Wilms Floet, P.A.Yagoubov, and E.L.Kollberg, IEEE Transactions on Microwave Theory and Techniques, **48**,600(2000)
15. W.J.Skocpol, M.R.Beasley and M.Tinkham, J.Appl. Phys. **45**, 4054(1974)
16. P.Khospropanah, H.Merkel, S.Yngvesson,A.Adam, S.Cherednichenko, and E.Kollberg, Proceedings of the 11th International Symposium on Space TeraHertz Technology, p. 474-488 (2000)

17. J.Ward, G.Chattopadhyay, A Maestrini, E.Schlecht, J.Gill, F.Maiwald, and L.Mehdi, Proceedings of the 15th International Symposium on Space Terahertz Technology, Northampton (MA), USA,April 2004
18. H.Pothier, S.Guéron,Norman O. Birge, D.Estève, and M.Devoret, Phys. Rev. Lett. **79**,3490(1997)
19. J.Seyler and M.N.Wybourne, Phys. Rev. Lett. **69**,1427(1992)
20. T.Klitsner, J.E.VanCleve, J.E.Fischer, and R.O.Pohl, Phys.Rev.**B38**, 7576(1988)
21. K.R.Patton and M.R.Geller, Phys. Rev.**B64**155320(2001)
22. D.H.Santamore and M.C.Cross, Phys. Rev.**B66**144302(2002)
23. K.Schwab, E.A.Henriksen, J.M.Worlock, and M.L.Roukes, Nature **404**974(2000)
24. M. Hajenius, J. J. A. Baselmans, J. R. Gao, T. M. Klapwijk, P. A. J. de Korte, B. Voronov and G. Gol'tsman, Superconducting Science and Technology, **17**, 224 (2004)
25. J.J.A.Baselmans, M.Hajenius,J.R.Gao,P.A.J. de Korte, T.M.Klapwijk, B.Voronov, and G.Golt́sman, this conference
26. E.M.Gershenson, G.N.Gol'tsman, A.I.Elant'ev, B.SD.Karasik, and S.E. Potoskuev, Sov. J.Low Temp. **14**,414(1988)
27. R.S.Nebosis, A.D.Semenov, Yu.P.Gousev, and K.F.Renk, Proceedings 7th International Symposium on Space TeraHertz Technology, University of Virginia, Charlottesvillem USA, p. 601
28. B.S. Karasik, B.Delaet, W.R.McGrath, J.Wei, M.E.Gershenson, and A.V.Sergeev, IEEE Transactions on Applied Superconductivity, **13**,188 (2003)